Applied Catalysis B: Environmental 322 (2023) 122118

Contents lists available at ScienceDirect

Applied Catalysis B: Environmental

journal homepage: www.elsevier.com/locate/apcatb

Mechanistic insights into the promotion of low-temperature NH_3-SCR catalysis by copper auto-reduction in Cu-zeolites

Dongdong Chen [a,1], Yaling Yan [b,1], Anqi Guo [a], Valentina Rizzotto [c], Huarong Lei [a,c], Zhiwei Qiao [b,*], Hong Liang [b], Magdalena Jabłońska [d], Xiangqiong Jiang [e], Jiuxing Jiang [e], Regina Palkovits [f], Peirong Chen [a,*], Daiqi Ye [a], Ulrich Simon [c]

[a] Guangdong Provincial Key Laboratory of Atmospheric Environment and Pollution Control, National Engineering Laboratory for VOCs Pollution Control Technology and Equipment, School of Environment and Energy, South China University of Technology, 510006 Guangzhou, China
[b] Guangzhou Key Laboratory for New Energy and Green Catalysis, School of Chemistry and Chemical Engineering, Guangzhou University, 510006 Guangzhou, China
[c] Institute of Inorganic Chemistry, RWTH Aachen University, Landoltweg 1a, 52074 Aachen, Germany
[d] Institute of Chemical Technology, Universität Leipzig, Linnéstr. 3, 04103 Leipzig, Germany
[e] MOE Key Laboratory of Bioinorganic and Synthetic Chemistry, School of Chemistry, Sun Yat-sen University, 510275 Guangzhou, China
[f] Chair of Heterogeneous Catalysis and Chemical Technology, RWTH Aachen University, Worringerweg 2, 52074 Aachen, Germany

ARTICLE INFO

Keywords:
Density-functional theory
In situ DRIFTS
In situ impedance spectroscopy
Molecular dynamics
XAS

ABSTRACT

The performance of Cu-chabazite (Cu-CHA) zeolite, the state-of-art catalyst for the ammonia-assisted selective reduction (NH_3-SCR) of toxic NO_x pollutants from heavy-duty diesel vehicles, is insufficient at low reaction temperatures and needs to be improved for meeting stringent emission regulations. Here, we demonstrate that the auto-reduction of isolated Cu sites (*i.e.* $Cu^{2+}[OH] \rightarrow Cu^{+}$) in Cu-CHA could promote the low-temperature NO_x abatement efficiency in NH_3-SCR. Combining *in situ* spectroscopy, steady-state/transient kinetic measurements and computational simulations, we unveiled that Cu auto-reduction, which was driven by non-oxidative thermal activation, weakened the Cu tethering to CHA framework and thus increased the Cu mobility, particularly, in the presence of NH_3. More importantly, auto-reduction-induced charge redistribution favored NO activation to form intimately interacted $Cu^{+}\cdots NO^{+}$ pairs, which enabled alternative and highly efficient pathways leading to drastically promoted NO abatement at temperatures below 250 °C. These mechanistic findings shed new light on tuning the speciation of Cu single-sites to promote NO_x reduction catalysis over Cu-zeolites.

1. Introduction

Copper-exchanged small-pore chabazite zeolites (Cu-CHA, including Cu-SAPO-34 and Cu-SSZ-13) are employed as the state-of-art catalysts in the ammonia-assisted selective catalytic reduction (NH_3-SCR) of harmful nitrogen oxides (NO_x) from heavy-duty diesel vehicles [1–3], because of their high activity, high selectivity to desired products (N_2), and excellent (hydro-)thermal stability under harsh conditions. While Cu-CHA has been proved to be highly active in NH_3-SCR in the temperature range 250–450 °C, its activity below 250 °C is insufficient to secure high NO_x abatement efficiency under cold-start conditions [4,5]. Enormous efforts were thus devoted to the mechanistic understanding of NO_x reduction over Cu-CHA catalysts [5–7], aiming at improving the low-temperature NH_3-SCR performance to meet the continuously tightening emission regulations. While important progress has already been achieved in the identification of catalytically active Cu sites and elementary reaction steps, much of the recent research focus shifts to the molecular understanding and delicate modulation of reaction-driven dynamic Cu speciation during NH_3-SCR at low temperatures [5,8].

In the CHA framework, Brønsted acid sites, which are generated by the substitution of P by Si (in SAPO-34) or of Si by Al (in SSZ-13), serve as coordination sites for the exchanged Cu ions [3,9,10]. Extensive investigations combining synchrotron-based *in situ* or *operando* spectroscopy and advanced computational simulations unveiled that the coordinative environment and the oxidation state of Cu sites change dynamically under reaction conditions [3,11]. Specifically, divalent Cu species, *i.e.,* Cu^{2+} located in the six-membered ring (6MR) and $Cu^{2+}[OH]$ located in the eight-membered ring (8MR), can be easily

* Corresponding authors.
E-mail addresses: zqiao@gzhu.edu.cn (Z. Qiao), chenpr@scut.edu.cn (P. Chen).
[1] These authors contributed equally.

https://doi.org/10.1016/j.apcatb.2022.122118
Received 10 August 2022; Received in revised form 24 October 2022; Accepted 25 October 2022
Available online 29 October 2022

reduced to monovalent Cu^+ by co-adsorbed NO and NH_3 molecules, and Cu^+ species can be re-oxidized (to Cu^{2+} or Cu^{2+}[OH]) by NO+O_2 or NO_2 to complete a catalytic/redox cycle [5,12]. Recent studies revealed that a fraction of hydroxylated Cu^{2+} species (Cu^{2+}[OH] in 8MR) in Cu-CHA zeolites undergo so-called "auto-reduction" or "self-reduction" (*i.e.*, hydroxylated Cu^{2+} species are reduced to Cu^+) upon thermal treatment in vacuum, inactive (*i.e.,* oxygen-free) or even oxidative atmospheres [13–15]. By monitoring the dehydration and activation processes with X-ray absorption and emission spectroscopies (XAS/XES), Borfecchia and co-authors revealed that activation in helium at 400 °C led to a loss of extra-ligands (*i.e.,* -OH) and eventually the auto-reduction of Cu^{2+}[OH] to Cu^+ [14]. Electron paramagnetic resonance spectroscopy studies found that Cu^{2+}[OH] can be reduced to Cu^+ in helium atmosphere at a temperature as low as 250 °C after prolonged treatment for 14 h [16]. A recent study combining *in situ* XAS and mass spectrometry confirmed that the intrinsic auto-reduction of Cu^{2+} species is associated with the release of oxygen and begins at temperatures higher than 400 °C [17].

Yet, little is known about the impact of Cu auto-reduction in NH_3-SCR catalysis. There is an assumption that NO_x reduction may be deteriorated by a loss of Cu^{2+}[OH] species, which are catalytically active in NH_3-SCR [16]. On the other hand, density-functional theory (DFT) and *ab initio* molecular dynamics (AIMD) simulations suggest that Cu ions (including Cu^{2+}, Cu^{2+}[OH] and Cu^+) are solvated and mobilized by NH_3 molecules at low temperatures (below 250 °C), and Cu^+ has a much higher mobility than Cu^{2+} or Cu^{2+}[OH] under similar solvating conditions (NH_3-solvated or non-solvated) [4,5,18]. During NH_3-SCR, the NH_3-solvated Cu^+, *i.e.,* $Cu^+(NH_3)_2$, can diffuse to neighboring CHA cages through the 8MR windows to form transient Cu ion pairs, which play a key role in the $Cu^+ \rightarrow Cu^{2+}$ re-oxidation at low temperatures [4]. In this regard, Cu auto-reduction may be beneficial for NH_3-SCR, in particular at low temperatures.

Here, we combine *in situ* spectroscopy, MD/DFT simulations and reaction kinetics to elucidate the role of Cu auto-reduction in NH_3-SCR catalysis over a commercially relevant Cu-CHA catalyst (*i.e.,* Cu-SAPO-34). Specifically, we applied *in situ* diffuse reflection infrared Fourier transform spectroscopy with NO or NH_3 as probe molecule (*in situ* NO-DRIFTS or NH_3-DRIFTS), supplemented with X-ray absorption near-edge spectroscopy (XANES) and extended X-ray absorption fine-structure spectroscopy (EXAFS), to probe the thermal activation-induced Cu^{2+}[OH]→Cu^+ auto-reduction. Impedance-based *in situ* modulus spectroscopy was then employed to reveal the change of Cu mobility (thereby the Cu-framework interaction) by auto-reduction. In NH_3-SCR catalysis, Cu auto-reduction favored the formation of reactive NO^+ species as $Cu^+ \cdots NO^+$ adducts, which enabled alternative and highly efficient NO abatement pathways at temperatures below 250 °C. Similar promotion of NH_3-SCR catalysis by Cu auto-reduction was also observed over other Cu-zeolites, namely Cu-SSZ-13 and Cu-ZSM-5.

2. Experimental

2.1. Catalyst preparation

The Cu-SAPO-34 catalyst was obtained by calcining commercial Cu-SAPO-34 powders (supplied by Clariant, Germany) at 500 °C for 2 h in static air. H-SSZ-13 zeolite (CHA-type framework, Si/Al=12.5) was synthesized following the same procedure as reported in literature [19]. Cu-SSZ-13 was synthesized by a wet ion-exchange method, and Cu^{2+} ions were supplied by aqueous solutions of $Cu(NO_3)_2{\cdot}3H_2O$ (≥99.5 %, Merck, Darmstadt, Germany). Specifically, the temperature of Cu ion exchange procedure was kept at 80 °C, which is favorable for the ion diffusion into the small-pore framework [19]. Before being dried in an oven at 100 °C overnight, the zeolite was recovered and washed with ultra-pure water for several times. The dried Cu-SSZ-13 was calcined at 500 °C for 2 h after full grinding. Cu-ZSM-5 with a Cu loading of 2 wt% was synthesized by aqueous ion exchange using commercially available H-ZSM-5 zeolite (Si/Al ~ 19, Nanjing XFNANO Materials Tech Co., Ltd) following the protocol described elsewhere [3]. The materials were recovered by filtration after ion exchange, thoroughly washed with distilled water (three times), and dried at 100 °C overnight. The obtained samples were then calcined at 550 °C for 4 h in flowing air in a furnace (Anhui Kemi Machinery Technology Co., Ltd). The ion exchange procedure was repeated for two times before calcination for increased Cu ion exchange levels.

2.2. Catalyst characterization

The physicochemical properties of the Cu-SAPO-34 and Cu-SSZ-13 catalysts were examinined by X-ray diffraction (XRD), N_2-physisorption, scanning electron microscopy (SEM), UV–visible diffuse reflection spectroscopy (DR UV/Vis), temperature programmed desorption using ammonia or oxygen as a probe molecule (NH_3-TPD/O_2-TPD), *in situ* diffuse reflectance infrared Fourier transform spectroscopy (DRIFTS), *in situ* impedance spectroscopy (IS) and X-ray absorption fine structure (XAFS) spectroscopy. The specific characterization procedures are discussed in detail in the Supplementary Information.

2.3. Steady-state and transient NH_3-SCR tests

Steady-state NH_3-SCR reactions were conducted under atmospheric pressure in a fixed-bed micro-reactor, whose inner diameter and total length are 6 mm and 320 mm, respectively. A FTIR gas analyzer (MKS 6030) was directly connected to the reactor through a heated stainless-steel tube, which can continuously monitor the reactant concentrations. Two sets of NH_3-SCR tests were conducted under different conditions as the following:

1) The inlet gas was composed of 300 ppm NO, 300 ppm NH_3, 7 vol% O_2, and N_2 as the balance gas, and the weight hourly space velocity (WHSV) was *ca.* 240,000 $ml{\cdot}h^{-1}{\cdot}g^{-1}$ (a total flow rate of 200 ml min^{-1}). 50 mg of catalyst was applied in each test and was outgassed in a flow of 10.0 vol% O_2/N_2 or pure N_2 (80 ml min^{-1}) at 450 °C for 2 h before NH_3-SCR reactions. The NH_3-SCR tests were also repeated in presence of ~1 vol% or ~10 vol% H_2O in the reaction mixture.
2) The inlet gas was composed of 2500 ppm NO, 2500 ppm NH_3, 2.5 vol % O_2, and Ar as the balance gas, and the WHSV was about 24,000 $ml{\cdot}h^{-1}{\cdot}g^{-1}$ (a total flow rate of 40 ml min^{-1}). The pre-treatment procedure was identical as the first set except the quantity of catalyst was 100 mg. It is worth noting that Ar instead of N_2 was used in catalytic tests to avoid any influence of the inlet N_2 on the monitoring of N_2 selectivity in NH_3-SCR.

Transient NH_3-SCR experiments were carried out at 50 °C or 100 °C. The pre-activated Cu-SAPO-34 (at 450 °C, in O_2 or Ar, 2 h) was first exposed to a gas stream containing 300 ppm NO or 10 vol% O_2 + 300 ppm NO (Ar balance) for 2 h, and then purged in pure Ar for 5 min. Afterwards, a gas stream containing 300 ppm NH_3 (Ar balance) was fed to the Cu-SAPO-34 catalyst, and the effluents were monitored continuously using an online mass spectrometer.

2.4. Computation details

The zeolite structures were optimized by density-functional theory (DFT) calculations using the ABINIT software package [20]. To represent the core-valence interactions, the calculations were performed spin-polarized using the projector augmented wave (PAW) method with Perdew-Burke-Ernzerhof (PBE) exchange-correlation functionals [21] and a cutoff energy of 400 eV was set for the plane wave. PAW-PBE calculation including Grimme's D3 dispersion correction [22] was carried out to take long-range van der Waals (vdW) interactions into account. To provide microscopic insight into the positions of restricted Cu atoms in the zeolite, molecular dynamics (MD) simulation were

Table 1
Lennard Jones parameters.

Atoms	Cu	Al	N	O	P	Si	H
σ (Å)	3.11	4.01	3.26	3.12	3.69	3.83	2.57
ε/k_B(K)	2.52	254.09	34.72	30.19	153.46	202.27	22.14

conducted to estimate the dynamic behavior of restricted Cu atoms in Cu-SAPO-34. All atoms of Cu-SAPO-34 were described by the Lennard-Jones (LJ) and electrostatic potentials. The LJ potential parameters in Table 1 were adopted from the universal force field [23] and the atomic charges of Cu and zeolite were estimated using the Qeq method [24]. To calculate the dynamic behavior of restricted Cu atoms in each 6MR, all structures were first optimized by the Forcite in Materials Studio. Then, each MD simulation at different temperatures was performed for 15 ns, and the temperature of simulation varied from 298 K to 798 K with an interval of 50 K, respectively. The SAPO-34 structure was assumed to be rigid during this simulation, but all Cu atoms in SAPO-34 were flexible. The positions of restricted Cu atoms in Cu-SAPO-34 and the radial distribution function (RDF) curves were estimated for the final structures after MD simulation. All of LJ interactions were evaluated with a cutoff of 12 Å, and the electrostatic interactions were estimated using the Ewald summation method with an accuracy of 10^{-3} kcal/mol.

The adsorption and transformation of NO in SCR reactions over Cu-SAPO-34 catalysts were simulated with the Heyd−Scuseria−Ernzerhof (HSE06) functional [25] in the Vienna *ab initio* simulation package (VASP) [26]. The project-augmented wave (PAW) [21] and D3 correction [22] methods were used to represent the core-valence interaction and van der Waals (vdW) interactions, respectively. Before the calculation, geometrical optimization was first carried out using the Perdew−Burke−Ernzerhof (PBE) functional [27], and all atoms were fully relaxed until the forces were lower than 0.05 eV/Å. Then HSE06 functional was employed to obtain the accurate total energy. For the calculations of total energy, a cutoff energy of 400 eV was set for plane wave basis sets to expand the valence electronic states, and spin polarization was included [28].

3. Results and discussion

3.1. Spectroscopic verification of Cu auto-reduction

According to XRD, N_2-physisorption and SEM studies, textural properties and morphology of Cu-SAPO-34 were not essentially modified by either the atmosphere-varied thermal treatments or the NH_3-SCR tests (Figs. S1–S4 in Supporting Information). DR UV/Vis examinations demonstrate that the charge transfer bands appeared mainly at wavelengths below 300 nm in both the O_2- and N_2-activated Cu-SAPO-34 (Fig. S3), confirming a predominant presence of isolated Cu species in the zeolite [3]. No CuO_x reflection was detected by XRD (Fig. S1a), in good agreement with the DR UV/Vis evidence showing the absence of CuO_x clusters in the sample (Fig. S3) [3].

Comparative *in situ* NO-DRIFTS and NH_3-DRIFTS investigations were performed to probe Cu auto-reduction in Cu-SAPO-34, and the time-

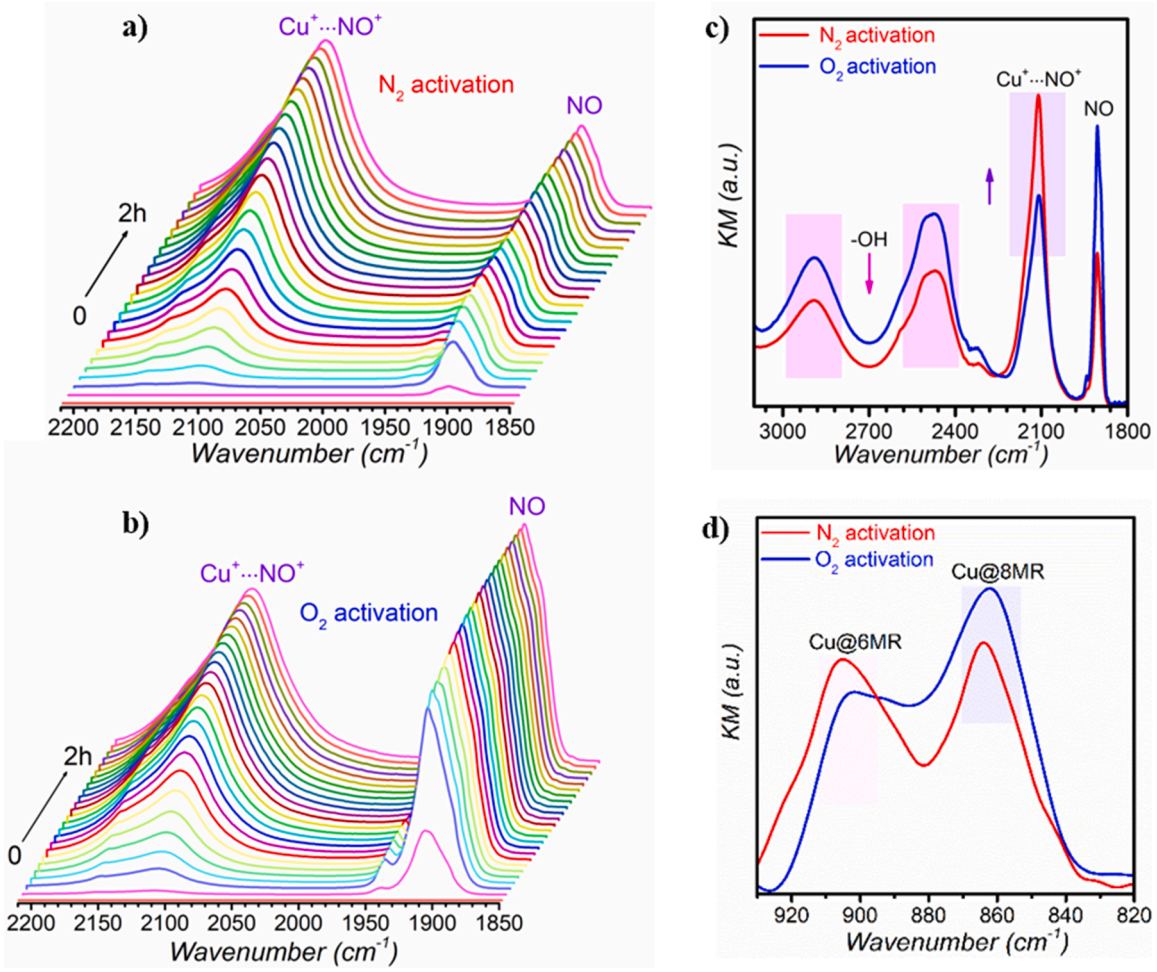

Fig. 1. Probing Cu auto-reduction by *in situ* DRIFTS. Time-resolved *in situ* DRIFT spectra of NO adsorption on a) N_2-activated and b) O_2-activated Cu-SAPO-34. A comparison of the *in situ* DRIFT spectra of Cu-SAPO-34 after saturation with c) NO and d) NH_3.

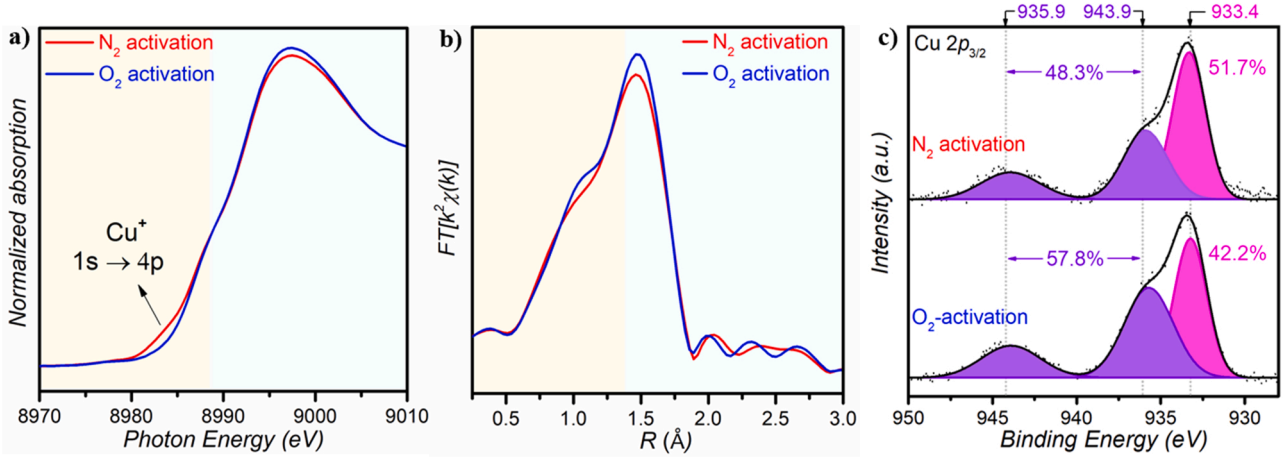

Fig. 2. Probing Cu auto-reduction by *ex situ* XAS and *quasi in situ* XPS. A comparison of the *ex situ* a) XANES and b) EXAFS spectra for Cu-SAPO-34 activated in N_2 (red) or in O_2 (blue). c) Deconvoluted *quasi in situ* XP Cu $2p_{3/2}$ spectra for N_2-activated (upper) and O_2-activated (bottom) Cu-SAPO-34.

resolved spectra of NO adsorption are displayed in Figs. 1a and b for Cu-SAPO-34 after thermal activation in N_2 and O_2, respectively. In both cases, stretching vibrations of adsorbed NO species, including NO molecules bounded on divalent Cu sites (at 1910 cm^{-1}) and NO^+ species (at 2130 cm^{-1}) [29,30], were observed and increased simultaneously with time until saturation. Fig. 1c compares the *in situ* DRIFT spectra (in the range 3100–1800 cm^{-1}) recorded over NO-saturated Cu-SAPO-34 samples. Intensities of the broad bands from 3200 to 2100 cm^{-1}, arising from H-bonded hydroxyl species [14], are significantly lower in N_2-activated Cu-SAPO-34, pointing to a loss of OH-ligands by high-temperature activation in N_2. This is believed to be associated with Cu auto-reduction *via* the following route [31].

$$2Cu^{2+}[OH] \rightarrow [Cu\text{-}O\text{-}Cu]^{2+} + H_2O \rightarrow 2Cu^{+} + 0.5O_2 + H_2O \quad (1)$$

Notably, the 1910 cm^{-1} band for NO bounded to divalent Cu was significantly lowered in intensity after thermal activation in N_2. Considering that Cu^{2+} sites are not influenced by the applied atmosphere (O_2 or N_2) during thermal activation [10], the decrease of band intensity at 1910 cm^{-1} can be attributed to a lower prosperity of $Cu^{2+}[OH]$ sites in the sample [14,32,33]. Interestingly, a significant increase in intensity at *ca.* 2130 cm^{-1} was observed over N_2-activated Cu-SAPO-34 (Fig. 1c), implying a more favorable activation of NO to NO^+ after auto-reduction [29,30].

As revealed previously, NO^+ species can be formed *via* the reduction of Cu^{2+} in 6MR by adsorbed NO (*i.e.*, $Cu^{2+} + NO \rightarrow Cu^{+}\text{-}NO^{+}$) [29,30]. Obviously, additional formation route should exist in N_2-activated Cu-SAPO-34, which lost part of its divalent Cu sites due to the preceding Cu auto-reduction [13]. According to Hadjiivanov et al. [34], NO^+ can be generated easily even on Cu-free proton-form zeolites, as a consequence of charge transfer from NO molecule to cationic sites on the zeolite framework. Recent spectroscopic and theoretical studies also revealed that NO^+ species can occupy cationic positions in close proximity of Cu^+ ions by forming $Cu^{+}\cdots NO^{+}$ complexes to compensate negative framework charge [29,35]. Therefore, it is more reasonable to attribute the increased band intensity at *ca.* 2130 cm^{-1} to additional NO^+ species that are hosted or stabilized by Cu^+ sites, *i.e.*, $Cu^{+}\cdots NO^{+}$ pairs [29,30]. Notably, the $Cu^{+}\cdots NO^{+}$ band reached saturation at a much slower pace than the NO band in both N_2- and O_2-activated Cu-SAPO-34 samples (Fig. S5), likely originating from a weaker adsorption strength of NO^+ on cationic sites than NO adsorbed directly on Cu^{2+} or $Cu^{2+}[OH]$ sites, which is consistent with that observed over Cu-SSZ-13 [29,30,35]. Characteristic band for NO bounded to Cu^+ species (at *ca.* 1800 cm^{-1}) [17] was not observed in both cases, likely due to an easier occupation of the Cu^+ sites by NO^+ in the Cu-SAPO-34 catalyst [30]. We also conducted *in situ* NH_3-DRIFTS to examine the speciation of Cu sites by thermal activation in different atmospheres. As demonstrated in Fig. 1d, two bands at *ca.* 860 and 905 cm^{-1} were observed in the spectra, and can be attributed to internal asymmetric framework T-O-T vibrations perturbed by Cu species located in 8MRs and 6MRs (denoted as Cu@6MR and Cu@8MR), respectively [36–38]. Clearly, thermal treatment in the inert atmosphere led to a decrease of the 860 cm^{-1} band and, meanwhile, an increase of the 905 cm^{-1} band, pointing to Cu migration from 8MRs to 6MRs after auto-reduction [13,38]. Such Cu reduction-induced modification of spectroscopic fingerprints, namely the trade-off change of band intensities at *ca.* 905 cm^{-1} and *ca.* 860 cm^{-1}, was also confirmed in a recent study by Millan et al. using DFT/AIMD simulations and *in situ* FTIR spectroscopy [13,38].

Furthermore, XAS was also employed to differentiate the oxidation state and coordination of Cu in Cu-SAPO-34 samples that were treated *ex situ* in N_2 or O_2. The Cu K-edge XANES spectra in Fig. 2a reveal a higher intensity at 8983 eV (corresponding to the $1s \rightarrow 4p$ transitions of Cu^+ ions) in N_2-activated Cu-SAPO-34, suggesting the presence of more Cu^+ in the sample [5,14]. In the EXAFS spectra (Fig. 2b), a decreased intensity of the first-shell peak at 1.5 Å was observed in case of N_2-activated Cu-SAPO-34, which is due to a loss of OH-ligands in the first coordination shell of Cu sites [5,10,14]. This evidence of lower Cu coordination is consistent with the observation of OH-ligand loss by *in situ* NO-DRIFTS (Fig. 1c). Cu auto-reduction and the related OH-ligand loss were also detected in temperature-programmed desorption (TPD) studies using O_2 or NH_3 as a probe molecule (see Fig. S6 and related discussions) [39].

Notably, the *ex situ*-treated Cu-SAPO-34 samples, although handled with care, were transferred in air without special protection prior to XAS measurements. A considerable amount of H_2O may be adsorbed by the auto-reduced Cu-SAPO-34 from ambient atmosphere [14], hindering the quantification of actual Cu^+ amount based on the collected XAS results. Therefore, *quasi in situ* XPS measurements were conducted over the N_2-activated Cu-SAPO-34, in order to avoid interference from adsorbed H_2O and to estimate the change of Cu^+ fraction after Cu auto-reduction. As demonstrated in the deconvoluted Cu $2p_{3/2}$ spectra (Fig. 2c), intensity of the characteristic peak at *ca.* 933.4 eV for Cu^+ increased slightly, whereas those for the characteristic peak at *ca.* 935.9 eV and the satellite peak at *ca.* 943.9 eV (both related to divalent Cu species) decreased [40], in the N_2-activated Cu-SAPO-34. Further quantitative analysis based on peak area integration [40] (see Supporting Information for more details) revealed a 9.5 % increase of Cu^+ concentration (meanwhile a 9.5 % decrease of divalent Cu) in the N_2-activated Cu-SAPO-34, in comparison with the sample activated in O_2. It has to be noted that a fraction of divalent Cu ions may be reduced by the X-rays during XPS measurements [40]. Meanwhile, the highly mobile Cu^+

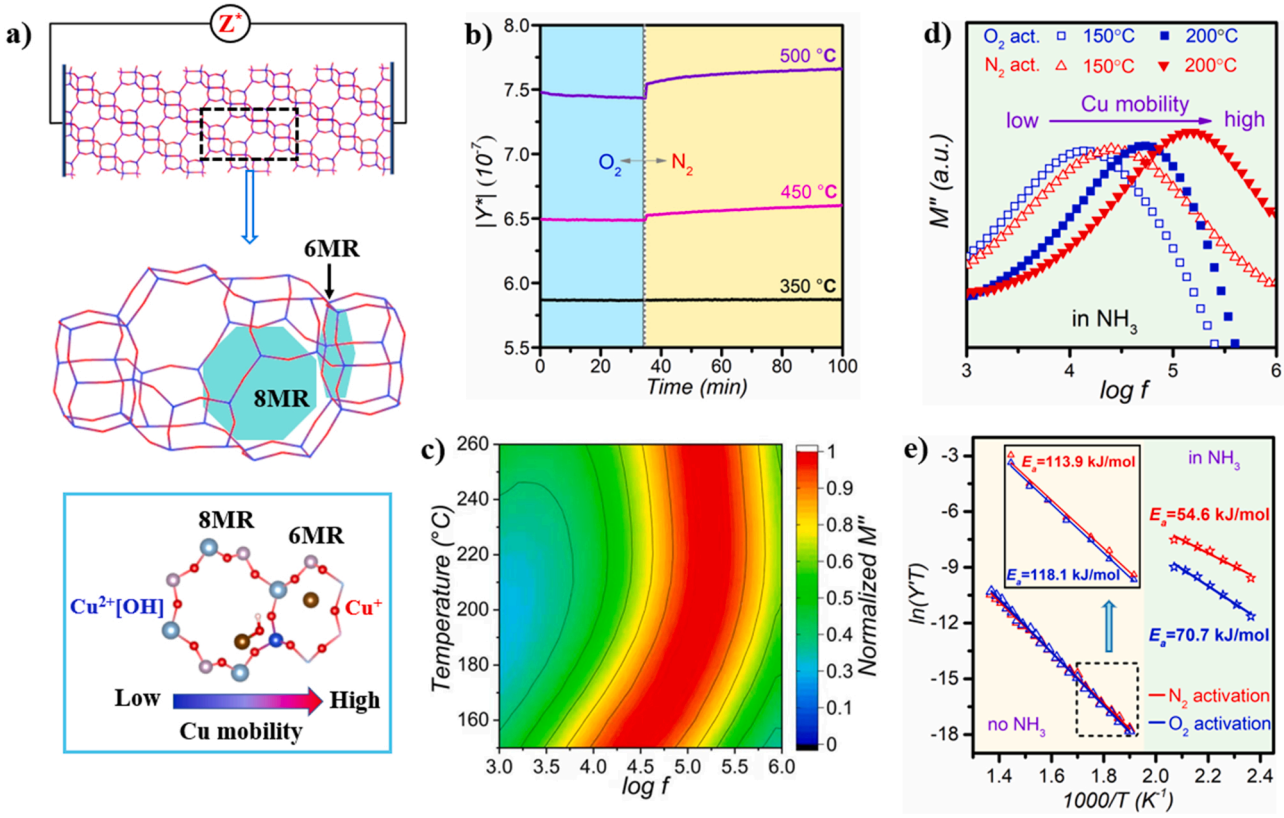

Fig. 3. Probing Cu mobility by *in situ* IS. a) Schematic illustration for *in situ* IS monitoring of Cu mobility within Cu-SAPO-34. b) Admittance $|Y^*|$ ($|Y^*| = 1/|Z^*|$) of Cu-SAPO-34 exposed to O_2 and N_2 in sequence. c) Temperature-dependent modulus spectra (high-frequency part) for N_2-activated Cu-SAPO-34 in flowing NH_3. d) Modulus spectra for Cu-SAPO-34 exposed to NH_3 at 150 °C and 200 °C. e) Arrhenius plots of Cu mobility and derived activation energies (E_a) for NH_3-solvated and non-solvated Cu-SAPO-34; E_a values are for Cu motion in the temperature range 150–210 °C in case of NH_3-solvated Cu-SAPO-34, and in the temperature range 250–450 °C in case of non-solvated Cu-SAPO-34); inset shows the enlarged Arrhenius plots for non-solvated Cu-SAPO-34. The *ln (Y'T)* values are based on the IS data at HF resonance frequencies determined in modulus spectra, and the E_a values were derived from the linear fitting of *ln (Y'T)* data.

species tend to migrate into the bulk of zeolite particles, instead of residing on the zeolite surface, and thus are less accessible by surface-sensitive techniques such as Total Electron Yield NEXAFS or XPS [41]. These two factors lead to unavoidable uncertainties in the quantification of different Cu species by *quasi in situ* XPS. Bulk-sensitive methods, such as *in situ* XAS, are thus required to obtain a more precise estimation of the actual Cu^+ content in the auto-reduced Cu-SAPO-34 catalyst.

Alteration of oxidation state is known to change the interactions between the Cu site and the CHA framework (more specifically, the electrostatic tethering of Cu to the zeolite matrix) and, consequently, the Cu mobility which affects greatly the low-temperature NH_3-SCR catalysis [4,5]. We thus applied *in situ* IS to examine the impact of auto-reduction on the Cu mobility within Cu-SAPO-34 (see measuring principles illustrated in Fig. 3a and zeolite micrographs in Fig. S7) [42]. As demonstrated previously [43], the distinct ion motion processes within Cu-zeolite catalysts can be resolved and visualized in the homologous spectral representation of the imaginary part of modulus M'' [3,44], which is defined as:

$$M'' = 2\pi f C_0 Z' \quad (2)$$

wherein f, C_0 and Z' represent the perturbing frequency, the capacity of the empty capacitor (*i.e.*, the geometric capacitance) and the real part of the complex impedance Z^* (see Fig. S8 for the measured Z' values), respectively [3]. As shown in Figs. S9 and S10, there are two well-separated resonance peaks in the modulus spectra collected at high temperatures under N_2 or O_2 atmosphere, corresponding to two distinct relaxation processes, namely the high-frequency (HF; $10^3 \sim 10^6$ Hz) one for the short-range (fast) ion motion or the local dipolar reorientation, and the low-frequency (LF; $10^{-1} \sim 10^3$ Hz) one for the long-range (slow) ion motion across zeolite lattice, respectively [44–46].

In N_2 atmosphere, an obvious shift of resonance peaks to higher frequencies (as compared to those measured in O_2 atmosphere) was observed at 400 °C and above (Figs. S9 and S10), suggesting that the relaxation time for ion motion was shortened (corresponding to an increased ion mobility) [3]. Noteworthy, such a frequency shift of resonance peaks was not recorded at 250 °C (Fig. S9a) and 350 °C (Fig. S9b). Similar phenomenon, *i.e.,* temperature- and atmosphere-dependent resonance peaks, was observed in Cu-SSZ-13 as well (Figs. S11 and S12), but not in Cu-free H-SSZ-13 (Fig. S13). As demonstrated in Fig. 1, Cu^{2+}[OH] auto-reduction at high temperatures in N_2 led to Cu^+ ions that are more mobile [12], and, consequently, a high-frequency shift of the respective resonance peaks in the modulus spectra (Fig. S10). To achieve an increased time resolution, single-frequency admittance $|Y^*|$ ($|Y^*| = 1/|Z^*|$, with $|Z^*|$ the absolute value of the complex impedance Z^*) was used to evaluate the condition-dependent Cu mobility (in terms of ionic conductivity) of Cu-SAPO-34 [47]. Fig. 3b displays the characteristic electrical response ($|Y^*|$ *vs.* time) collected during exposure to O_2 and N_2 in sequence. At high temperatures (450 °C and 500 °C), the admittance of Cu-SAPO-34 is higher in N_2 than in O_2, corresponding to an increased Cu mobility [45]. On the contrary, such atmosphere-dependent Cu mobility was not observed at a lower temperature of 350 °C (Fig. 3b), confirming the observations in modulus spectra (Figs. S9 and S10) that the Cu mobility of Cu-SAPO-34 was indeed increased by the auto-reduction process at high temperatures in inert atmosphere. We further investigated the Cu mobility in auto-reduced Cu-SAPO-34 in flowing NH_3 atmosphere at low temperatures (150–260 °C) to mimic the NH_3-solvation condition in

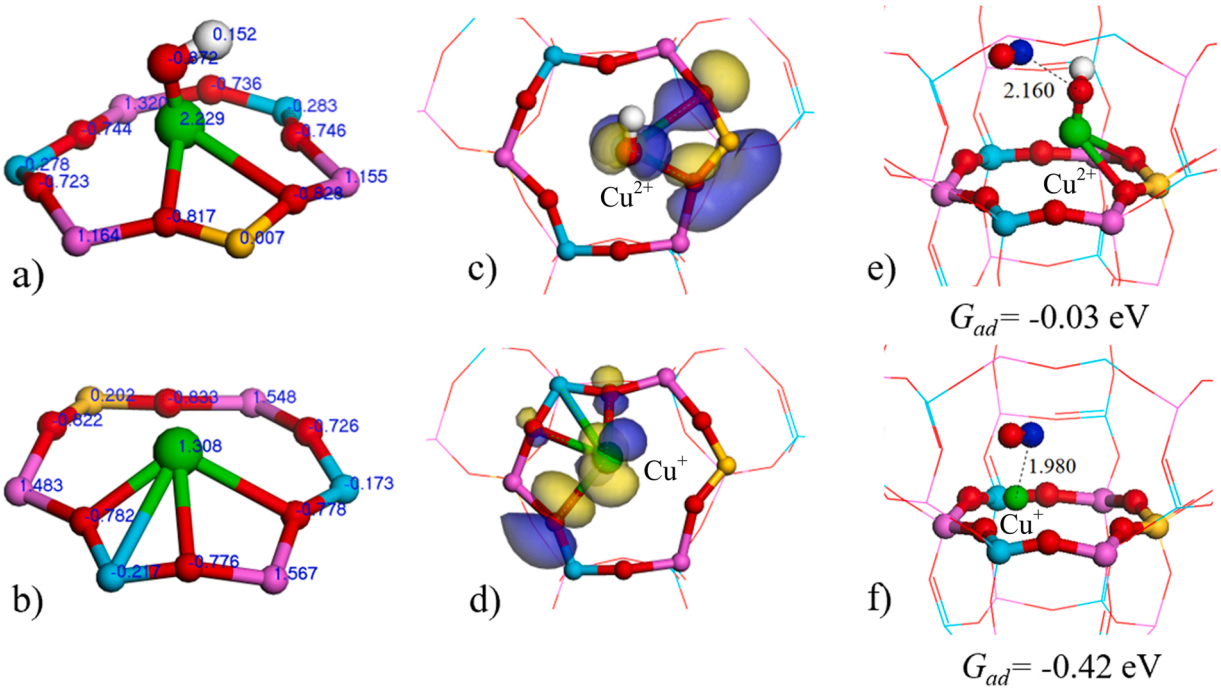

Fig. 4. Impact of Cu auto-reduction on NO activation. Charge numbers (a and b) and density distributions (c and d) of the 6MRs containing Cu^{2+}[OH] (a and c) and Cu^{+} (b and d). Yellow indicates electron accumulation, and blue indicates electron depletion. Structural illustrations for the Cu^{2+}[OH]···NO (e) and Cu^{+}···NO (f) adducts (the numbers are Cu-N distance in Å) by DFT calculation. Color codes: Cu-green, Si-yellow, O-red, N-blue, Al-pink, H-white, P-cyan. The charge calculations (a-d) were performed using the Qeq method, and the DFT calculations were run by the HSE06 functional. The charges of Cu ions in (e) and (f) are 2.108 and 1.133, respectively.

NH_3-SCR. As depicted by the modulus results (Fig. 3c and d), the HF peak of N_2-activated Cu-SAPO-34 in NH_3 shifted rapidly to higher frequencies with the increase of temperature from 150 to 210 °C and then slightly to lower frequencies from 210 to 260 °C, resulting in a maximum *log f* value of *ca.* 5.40, which is higher than the highest *log f* value (*ca.* 5.00) of O_2-activated Cu-SAPO-34 in NH_3. More clearly, a higher *log f* value was observed over N_2-activated Cu-SAPO-34 than the O_2-activated sample at each selected temperature (150 or 200 °C; Fig. 3d), corresponding to a higher mobility of the NH_3-solvated Cu sites [3]. Fig. 3e shows the quantified mobilities of non-solvated and NH_3-solvated Cu that were derived from a modified Arrhenius equation [48].

$$ln\ (YT) = A_0 - E_a / (k_B\ T) \quad (3)$$

wherein k_B, E_a and A_0 represent the Boltzmann constant, the activation energy for Cu ion motion and the pre-exponential factor (which is related to the type and number of the mobile ions), respectively [45,48]. *Y* represents the real part of the admittance Y^*, which was determined by the *log f* values of HF peaks in modulus spectra [49]. A higher *ln (YT)* value in Fig. 3e corresponds to a higher ionic conductivity, *i.e.* a higher Cu mobility within the zeolite [45,49]. In general, NH_3 solvation increased significantly the mobility of Cu in Cu-SAPO-34 and, meanwhile, decreased E_a for Cu ion motion, which is consistent with our previous study [45] and AIMD simulations in literature [5]. While auto-reduction moderately increased the Cu mobility under non-solvating conditions, the Cu mobility under NH_3-solvation conditions was significantly higher in auto-reduced Cu-SAPO-34 than in O_2-activated sample (Fig. 3e). Correspondingly, E_a for Cu ion motion was decreased considerably by auto-reduction (from 70.7 to 53.6 kJ/mol) under NH_3-solvation conditions. The effect of auto-reduction is less pronounced (from 118.1 to 113.9 kJ/mol) under non-solvating conditions, although it is indicative for the formation of highly mobile Cu^{I} species in N_2-activated Cu-SAPO-34 as well [4,5].

3.2. Impact of Cu auto-reduction on NO activation and reduction

Combined MD and DFT simulations were then performed to validate and supplement the *in situ* spectroscopic findings on Cu auto-reduction and Cu mobility. Final Cu positions in the auto-reduced Cu-SAPO-34 were estimated and optimized by NVT-MD simulations (*i.e.,* at constant number of atoms, with constant volume and temperature). As demonstrated in Fig. S14a, most of Cu atoms are located on the 6MR planes and at positions slightly off the 6MR centers, in accordance with previous DFT calculations [3]. The optimized local structure of Cu (Fig. S14b) demonstrates a strong bonding between the Cu and O atoms at the CHA framework, consistent with classical first-principles DFT simulations [4,5,7]. Aiming to verify the Cu auto-reduction effect (*i.e.,* the transformation of Cu^{2+}[OH] to Cu^{+}), we also carried out DFT calculations to estimate the charge valence number of each atom in the 6MR with Cu^{2+}[OH] or Cu^{+}. Comparing the final structures in Figs. 4a, b and S14c, we notice that the Cu location was changed clearly after auto-reduction, deviating from a position near the Si atom to a position near the P atom. The loss of OH-ligand in Cu^{2+}[OH] at high temperatures led to electron transfer to the Cu, which eventually reduced Cu^{2+} to Cu^{+}. The binding energies of Cu^{2+}[OH] and Cu^{+} in the 6MR of SAPO-34 were estimated by DFT to be − 0.16 eV and − 0.05 eV, respectively. The smaller binding energy value for Cu^{+} corresponds to a weaker Cu tethering to the zeolite lattice and a lower energy barrier for Cu motion within the CHA framework, and consequently results in a higher mobility of Cu sites as revealed by *in situ* IS (Fig. 3b and d) [4,5]. In view of the charge density distribution in Fig. 4c, there is a strong binding of Cu^{2+} with the framework O atoms, and a weak binding with the framework Si atom. After the loss of OH-ligand, the Cu^{+} ion was detached from the Si atom and moved to the vicinity of the P atoms (Fig. 4d). Charge density calculation revealed a change of Cu valence from 2.229 (Cu^{2+}[OH]) to 1.308 (Cu^{+}) after OH-ligand loss, respectively, indicating that 0.921 electron was donated from the OH-ligand to Cu^{2+}, that is, the Cu^{2+}[OH] was auto-reduced to Cu^{+}. Meanwhile, charge depletion was noticed on

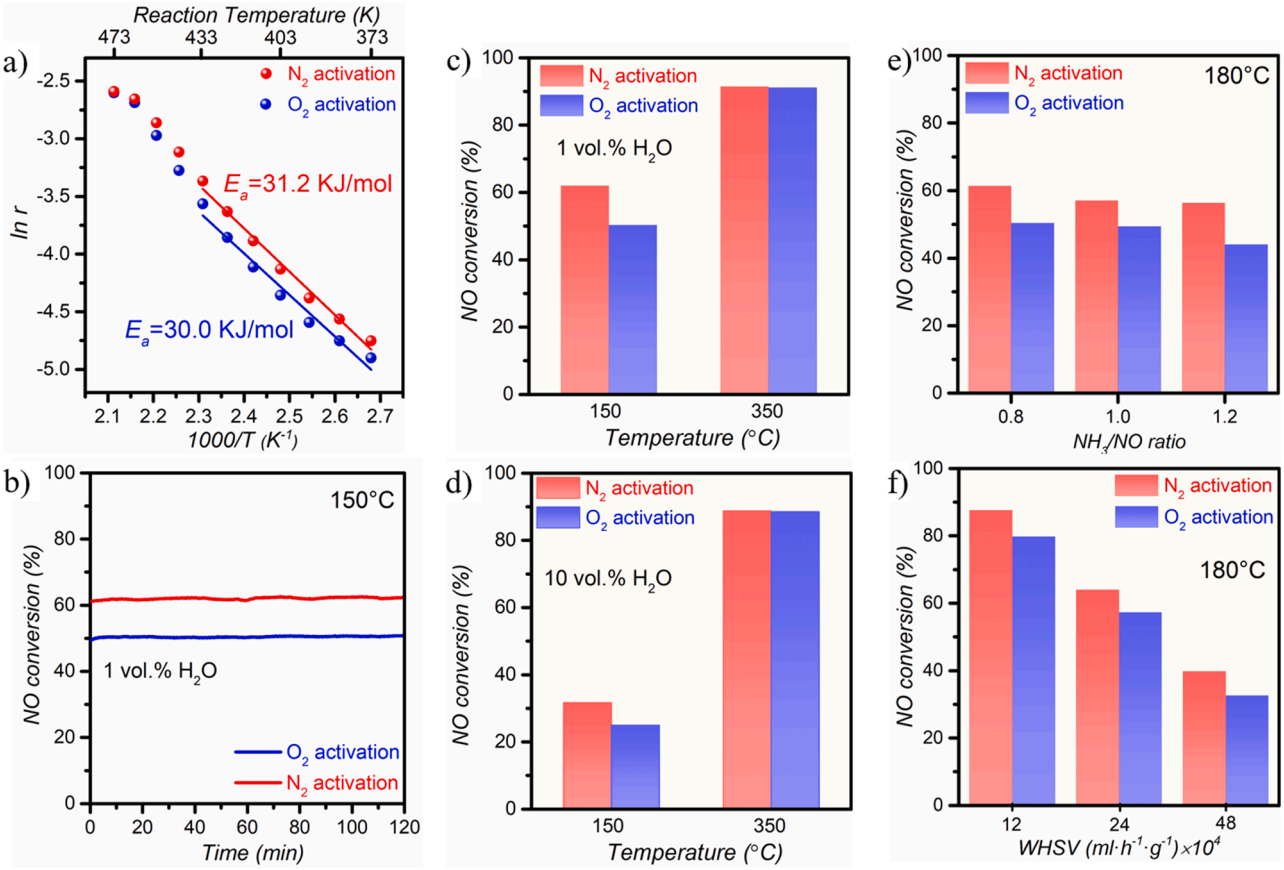

Fig. 5. Impact of Cu auto-reduction on NH_3-SCR catalysis. a) NO conversion rates in "dry" standard NH_3-SCR tests at low temperatures (100–300 °C). b) Time-on-stream NO conversions over Cu-SAPO-34 activated in different atmospheres at 150 °C. c) NO conversions (after two-hour time-on-stream) in "wet" NH_3-SCR tests with c) 1 vol% or d) 10 vol% H_2O in the reaction stream at fixed temperatures (150 °C and 350 °C). e) NO conversions at 180 °C in "dry" NH_3-SCR tests with different NH_3/NO ratios. f) NO conversions at 180 °C in "dry" NH_3-SCR tests with different weight hourly space velocities (WHSV).

three different O positions at the 6MR containing Cu^+, instead of two O positions in case of 6MR with Cu^{2+}[OH].

The charge redistribution induced by Cu auto-reduction also affected profoundly the configuration and strength of NO adsorption/activation on the Cu site. On the one hand, charge depletion led to additional cationic sites on the 6MR for the activation of NO to form intimately interacted $Cu^+\cdots$NO adduct (Fig. S15), coinciding with the formation of $Cu^+\cdots NO^+$ pairs as revealed by the *in situ* NO-DRIFTS studies of auto-reduced Cu-SAPO-34 (Fig. 1c). On the other hand, NO adsorption strength (as indicated by the absolute value of adsorption energy G_{ad}) is significantly higher on the Cu^+ ion and the cationic positions of auto-reduced Cu-SAPO-34 (Figs. 4 f and S15) than on the Cu^{2+}[OH] in case of pristine Cu-SAPO-34 (Fig. 4e). Notably, Cu^+ ions in the auto-reduced Cu-SAPO-34 could host NO species with a more negative G_{ad} value of − 0.42 eV (Fig. 4 f) than that of Cu^{2+}[OH] (Fig. 4e), and thus it could directly serve as the preferential sites for adsorbing NO and stabilize the reactive NO^+ species generated on the cationic sites at 6MR. Moreover, the shorter distance between Cu and N in the $Cu^+\cdots$NO adduct (1.98 Å) than in the Cu^{2+}[OH]$\cdots$NO adduct (2.16 Å), which indicates a more intimate coupling of NO and the auto-reduced Cu^+ site, further evidences the formation of $Cu^+\cdots NO^+$ pairs as observed by *in situ* NO-DRIFTS [29,30].

The role of Cu auto-reduction in NH_3-SCR catalysis was investigated basically by comparing the activities of Cu-SAPO-34 after activation in different atmospheres (oxidative or inert), under both "dry" (*i.e.* without H_2O vapor in the reaction mixture) and "wet" (*i.e.* with H_2O vapor) conditions (Figs. 5, S16–S20). Surprisingly, at the same temperature in the range of 100–160 °C, a higher NO conversion rate was achieved over N_2-activated Cu-SAPO-34 than the O_2-activated one in "dry" tests (Fig. 5a), pointing to a promotional effect of Cu auto-reduction in low-temperature NH_3-SCR catalysis. The calculated E_a values, *i.e.,* 31.2 kJ/mol and 30.0 kJ/mol for N_2- and O_2-activated Cu-SAPO-34 catalysts, respectively, are typical for NH_3-SCR over Cu-CHA catalysts with low Cu loadings [7,36]. Similarly, in "wet" tests (*i.e.* with 1 vol% or 10 vol% H_2O in the reaction mixture), higher NO conversions were achieved at 150 °C over Cu-SAPO-34 after activation in N_2 than that after activation in O_2 (Fig. 5b–d). Interestingly, such promoting effect was not observed at a higher temperature of 350 °C (Figs. 5c, d and S17), likely due to a change of the NH_3-SCR mechanism in which the adsorption and activation of NO on the zeolite catalyst is dispensable [7]. The pronounced promotional effect of Cu auto-reduction in NH_3-SCR was also observed in "dry" tests with drastically different gas compositions (in terms of NO/NH_3 ratio) (Figs. 5e and S18) and space velocities (Figs. 5f and S19), and in "wet" NH_3-SCR tests using a different experimental setup (Fig. S20). Moreover, as demonstrated in Fig. S20, the promoting effect of Cu auto-reduction in NH_3-SCR could last for more than 10 h at 200 °C without drastic decay. Similar improvement in low-temperature NH_3-SCR performance was also observed over N_2-activated Cu-SSZ-13 and Cu-ZSM-5 with respect to their O_2-activated counterparts (Fig. S21), confirming the promoting effect of Cu auto-reduction as a universal phenomenon for Cu-zeolites in NH_3-SCR catalysis.

3.3. Reaction mechanisms

It is well accepted that NH_3-SCR reactions take place over NH_3-solvated Cu ions in Cu ion-exchanged zeolites (including Cu-SSZ-13, Cu-SAPO-34, Cu-ZSM-5, Cu-Beta, *etc.*) at low temperatures (below 250 °C) [3,4,7,15]. According to Millan et al. [38], the solvation effect of NH_3

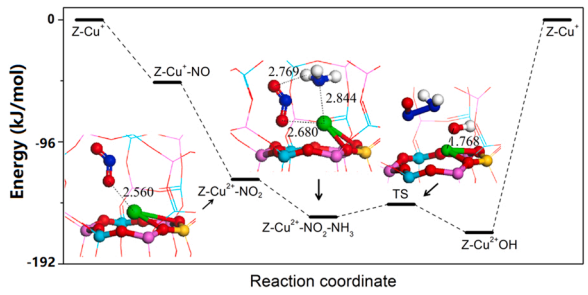

Fig. 6. Mechanistic investigation by DFT simulations. Cu local structures and free energies along the standard NH_3-SCR reaction pathway over the auto-reduced Cu-SAPO-34 (denoted as Z-Cu^+) by DFT-HSE06 calculations (green, yellow, red, pink, cyan, blue and white spheres indicate Cu, Si, O, Al, P, N and H atoms, respectively). The DFT calculations were run by HSE06 functional. The charges of Cu ions are 1.983 for Z-Cu^{2+}-NO_2, 2.033 for Z-Cu^{2+}-NO_2-NH_3 and 1.977 for TS, respectively.

can result in the disappearance of all Cu-perturbated T-O-T vibration bands in the range of 800–1000 cm^{-1}, due to Cu detachment from the zeolite framework. However, in the auto-reduced Cu-SAPO-34, these bands were still clearly observable in the NH_3-DRIFT spectra (Fig. 1d), indicating the presence of framework-coordinated Cu species in Cu-SAPO-34 even after NH_3 loading. Taking this evidence into account, we considered framework-coordinated Cu as the initial active sites for NO adsorption and activation over the auto-reduced Cu-SAPO-34 (denoted as Z-Cu^+), and proposed an alternative NH_3-SCR reaction route (Fig. 6) based on DFT interrogations. The negative free energy values suggest that all the involved reaction coordinates in Fig. 6 are thermodynamically favorable. Free energy penalty indicates that Z-Cu^+···NO^+ pair can be easily transformed to Z-Cu^{2+}-NO_2 upon interacting with O_2. Interaction between Z-Cu^{2+}-NO_2 and co-adsorbed NH_3 led to the formation of a Z-Cu^{2+}/NO_2NH_3 intermediate, which was transformed to a transition state (TS) of Cu^{2+}(OH)/H_2NNO with a moderate energy barrier of 9.984 kJ/mol [4,5,7]. After the release of H_2O and N_2 as products, the hydroxylated form of Cu site, namely Cu^{2+}[OH], was re-generated and can be transformed to Cu^+ by auto-reduction to complete the Cu redox cycle and the NH_3-SCR turnover cycle (Fig. 6).

The reaction pathway by DFT-HSE06 calculations was confirmed by *in situ* DRIFTS and transient catalytic experiments. As displayed in Fig. 7a and S22, enhanced intensities of IR bands for monodentate nitrate (1602–1612 cm^{-1}), adsorbed NO_2 (1625 cm^{-1}) and bidentate nitrates (1530 and 1576 cm^{-1}) were recorded during NO+O_2 adsorption on N_2-activated Cu-SAPO-34 samples owing to its improved NO oxidation ability (Fig. S23) [37]. Correspondingly, in the transient experiments of NH_3 exposure to Cu-SAPO-34 pre-saturated with NO and O_2, a much more pronounced N_2 signal at m/z 28 was detected over the Ar-activated Cu-SAPO-34 at 100 °C or even 50 °C (Figs. 7b and S24, upper parts), suggesting a promoted reaction between NH_3 and the adsorbed NO_2 or nitrate species to form N_2 molecules. Surprisingly, more favorable N_2 formation were also observed upon feeding NH_3 to auto-reduced Cu-SAPO-34 pre-treated by NO in the absence of O_2 (Figs. 5c and S24, bottom parts), which is likely due to another NO reduction pathway mediated by the highly reactive Cu^+···NO^+ pairs (Fig. S24) [50]. The less favorable N_2 formation on O_2-activated Cu-SAPO-34, observed during NH_3 exposure after NO or NO+O_2 pre-adsorption, confirms that NO^+ on cationic sites generated after Cu auto-reduction, rather than those formed *via* Cu^{2+}+NO interaction (Fig. 1), are the key species responsible for the promoted N_2 formation over N_2-activated Cu-SAPO-34. Notably, combining the schemes of Cu^{2+}[OH]→Cu^+ auto-reduction (Eq. 1) and of Cu^+→Cu^{2+}[OH] re-oxidation in Fig. 6, *i.e.*,

$$Cu^+ + NH_3 + NO + 0.5\ O_2 \rightarrow N_2 + H_2O + Cu^{2+}[OH] \quad (4)$$

leads to a stoichiometry fully consistent with the standard NH_3-SCR reaction (Eq. 5) [50], *i.e.*,

$$4\ NH_3 + 4\ NO + O_2 \rightarrow 4\ N_2 + 6\ H_2O \quad (5)$$

thus rationalizing the proposed reaction coordinates for NO^+-mediated low-temperature NH_3-SCR catalysis over auto-reduced Cu-SAPO-34. These NO^+-mediated pathways, as alternatives and supplements to the well-accepted NH_3-SCR cycle involving Cu^{2+}↔Cu^+ (Eqs. 6 and 7) and/or Cu^{2+}[OH]↔Cu^+ (Eqs. 8 and 4) redox cycles [3,5,12,28], are considered to be responsible for the facilitated NO_x reduction at low temperatures (Fig. 4).

$$Cu^{2+} + 2\ NH_3 + NO \rightarrow Cu^+ + NH_4^+ + N_2 + H_2O \quad (6)$$

$$Cu^+ + NH_4^+ + NO + 0.5\ O_2 \rightarrow Cu^{2+} + N_2 + 2\ H_2O \quad (7)$$

$$Cu^{2+}[OH] + NH_3 + NO \rightarrow Cu^+ + N_2 + 2\ H_2O \quad (8)$$

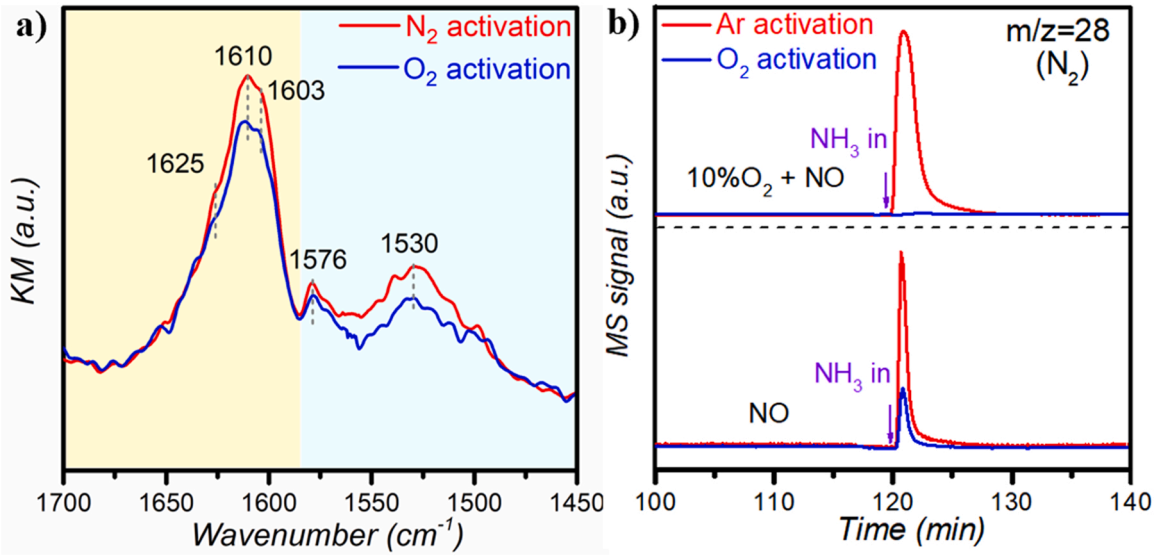

Fig. 7. Mechanistic investigation by ***in situ*** DRIFTS and transient experiments. a) *In situ* DRIFT spectra obtained after exposing the Cu-SAPO-34 samples to NO+O_2 at 100 °C. b) Evolution of N_2 (signal at m/z = 28 by online mass spectrometry) in transient experiments of NH_3 reaction with pre-adsorbed NO+O_2 (upper part) or NO (bottom part) over Cu-SAPO-34.

Based on this, future studies will be directed towards controllable interplay of enhanced Cu^+ mobility and $Cu^+\cdots NO^+$ formation. Furthermore, it is conceivable that NO^+ itself can get mobile as a charge compensating cation, as previously reported for alumina-based solid NO^+ conductors [51]. According to the experimental and theoretical findings (in this study and also in literature [35]) that NO^+ species occupy cationic positions in close proximity to Cu ions, one might assume that the NO^+ motion will be closely correlated to the motion of Cu^+ ions, which will be a novel aspect in further deciphering of the NH_3-SCR catalysis.

4. Conclusions

In summary, spectroscopic and theoretical interrogations of a small-pore CHA-type Cu-zeolite catalyst unveiled that Cu auto-reduction favored NO activation to form $Cu^+\cdots NO^+$ pairs and increased clearly the mobility of Cu sites. In low-temperature NH_3-SCR catalysis, an improved NO conversion was achieved over auto-reduced Cu-zeolites, which is attributed to NO^+-mediated alternative NO_x reduction pathways enabled by Cu auto-reduction. Our study provides new insights into the effect of Cu auto-reduction on the nature and reactivity of small-pore Cu-CHA zeolite in selective NO_x reduction catalysis, and may offer opportunities to understand mechanistically the role of Cu speciation in the general context of environmental catalysis over Cu-zeolites, such as NO or N_2O decomposition, NO_x reduction by hydrocarbons, CH_4 activation and conversion, *etc*.

CRediT authorship contribution statement

Dongdong Chen: Writing – original draft, Methodology. **Yaling Yan:** Methodology, Formal analysis. **Anqi Guo:** Writing – review & editing, Methodology. **Valentina Rizzotto:** Methodology. **Huarong Lei:** Methodology. **Zhiwei Qiao:** Funding acquisition, Writing – review & editing, Supervision. **Hong Liang:** Supervision. **Magdalena Jabłońska:** Methodology. **Xiangqiong Jiang:** Methodology. **Jiuxing Jiang:** Writing – review & editing, Supervision. **Regina Palkovits:** Writing – review & editing, Supervision. **Peirong Chen:** Funding acquisition, Writing – review & editing, Supervision. **Daiqi Ye:** Funding acquisition, Supervision. **Ulrich Simon:** Funding acquisition, Writing – review & editing, Supervision.

Declaration of Competing Interest

The authors declare that they have no known competing financial interests or personal relationships that could have appeared to influence the work reported in this paper.

Data availability

Data will be made available on request.

Acknowledgements

This work was supported by the National Natural Science Foundation of China (21976058, 21978058, 21971259), the Science and Technology Program of Guangzhou (202102080490), the National Engineering Laboratory for Mobile Source Emission Control Technology (NELMS2020A10), the Fundamental Research Funds for the Central Universities (2022ZYGXZR018), the Natural Science Foundation of Guangdong Province (2020A1515010800), and by the Cluster of Excellence "The Fuel Science Center" (EXC 2186, ID: 390919832) under the Excellence Initiative of the German federal and state governments to promote science and research at German universities. P.C. and Z.Q. appreciate the funding from the Pearl River Talent Recruitment Program of Guangdong Province. We thank Prof. Xingfu Tang (Fudan University) and Prof. Ralf Moos (University of Bayreuth) for inspiring discussions.

Supporting information

Catalyst characterization details; XRD, N_2-physisorption, SEM, DR UV/Vis, normalized DRIFTS and TPD (NH_3-TPD and O_2-TPD) results for Cu-SAPO-34; measured Z' and $-Z''$ values for Cu-SAPO-34 and Cu-SSZ-13; modulus plots for Cu-SAPO-34, Cu-SSZ-13 and H-SSZ-13; NVT-MD simulations and RDFs for local Cu structure; structural illustration of NO adsorption over Cu zeolites; kinetic results at varied NO/NH_3 ratios and WHSVs; NO oxidation curves; transient NH_3-SCR results and DRIFT spectra ($NO+O_2$ adsorption) for Cu-SAPO-34; steady-state NH_3-SCR results for Cu-SSZ-13 and Cu-ZSM-5.

Appendix A. Supporting information

Supplementary data associated with this article can be found in the online version at doi:10.1016/j.apcatb.2022.122118.

References

[1] E. Bello, P. Ferri, M. Nero, T. Willhammar, I. Millet, F.W. Schütze, L. van Tendeloo, P.N.R. Vennestrøm, M. Boronat, A. Corma, M. Moliner, NH_3-SCR catalysts for heavy-duty diesel vehicles: preparation of CHA-type zeolites with low-cost templates, Appl. Catal. B Environ. 303 (2022), 120928.
[2] N. Usberti, F. Gramigni, N.D. Nasello, U. Iacobone, T. Selleri, W. Hu, S. Liu, X. Gao, I. Nova, E. Tronconi, An experimental and modelling study of the reactivity of adsorbed NH_3 in the low temperature NH_3-SCR reduction half-cycle over a Cu-CHA catalyst, Appl. Catal. B Environ. 279 (2020), 119397.
[3] P. Chen, A. Khetan, M. Jabłońska, J. Simböck, M. Muhler, R. Palkovits, H. Pitsch, U. Simon, Local dynamics of copper active sites in zeolite catalysts for selective catalytic reduction of NO_x with NH_3, Appl. Catal. B Environ. 237 (2018) 263–272.
[4] C. Paolucci, I. Khurana, A.A. Parekh, S. Li, A.J. Shih, H. Li, J.R. Di Iorio, J. D. Albarracin-Caballero, A. Yezerets, J.T. Miller, W.N. Delgass, F.H. Ribeiro, W. F. Schneider, R. Gounder, Dynamic multinuclear sites formed by mobilized copper ions in NO_x selective catalytic reduction, Science 357 (2017) 898.
[5] C. Paolucci, A.A. Parekh, I. Khurana, J.R. Di Iorio, H. Li, J.D. Albarracin Caballero, A.J. Shih, T. Anggara, W.N. Delgass, J.T. Miller, F.H. Ribeiro, R. Gounder, W. F. Schneider, Catalysis in a cage: condition-dependent speciation and dynamics of exchanged Cu cations in SSZ-13 zeolites, J. Am. Chem. Soc. 138 (2016) 6028–6048.
[6] R. Villamaina, S. Liu, I. Nova, E. Tronconi, M.P. Ruggeri, J. Collier, A. York, D. Thompsett, Speciation of Cu cations in Cu-CHA catalysts for NH_3-SCR: effects of SiO_2/AlO_3 ratio and Cu-loading investigated by transient response methods, ACS Catal. 9 (2019) 8916–8927.
[7] F. Gao, D. Mei, Y. Wang, J. Szanyi, C.H.F. Peden, Selective catalytic reduction over Cu/SSZ-13: linking homo- and heterogeneous catalysis, J. Am. Chem. Soc. 139 (2017) 4935–4942.
[8] P.C. Bruzzese, E. Salvadori, S. Jäger, M. Hartmann, B. Civalleri, A. Pöppl, M. Chiesa, ^{17}O-EPR determination of the structure and dynamics of copper single-metal sites in zeolites, Nat. Commun. 12 (2021) 4638.
[9] D. Chen, H. Lei, W. Xiong, Y. Li, X. Ji, J.-Y. Yang, B. Peng, M. Fu, P. Chen, D. Ye, Unravelling phosphorus-induced deactivation of Pd-SSZ-13 for passive NO_x adsorption and CO oxidation, ACS Catal. 11 (2021) 13891–13901.
[10] E. Borfecchia, P. Beato, S. Svelle, U. Olsbye, C. Lamberti, S. Bordiga, Cu-CHA – a model system for applied selective redox catalysis, Chem. Soc. Rev. 47 (2018) 8097–8133.
[11] J. Becher, D.F. Sanchez, D.E. Doronkin, D. Zengel, D.M. Meira, S. Pascarelli, J.-D. Grunwaldt, T.L. Sheppard, Chemical gradients in automotive Cu-SSZ-13 catalysts for NO_x removal revealed by operando X-ray spectrotomography, Nat. Catal. 4 (2021) 46–53.
[12] C. Paolucci, A.A. Verma, S.A. Bates, V.F. Kispersky, J.T. Miller, R. Gounder, W. N. Delgass, F.H. Ribeiro, W.F. Schneider, Isolation of the copper redox steps in the standard selective catalytic reduction on Cu-SSZ-13, Angew. Chem., Int. Ed. 53 (2014) 11828–11833.
[13] C.W. Andersen, E. Borfecchia, M. Bremholm, M.R.V. Jørgensen, P.N. R. Vennestrøm, C. Lamberti, L.F. Lundegaard, B.B. Iversen, Redox-driven migration of copper ions in the Cu-CHA zeolite as shown by the insitu PXRD/XANES technique, Angew. Chem., Int. Ed. 56 (2017) 10367–10372.
[14] E. Borfecchia, K.A. Lomachenko, F. Giordanino, H. Falsig, P. Beato, A.V. Soldatov, S. Bordiga, C. Lamberti, Revisiting the nature of Cu sites in the activated Cu-SSZ-13 catalyst for SCR reaction, Chem. Sci. 6 (2015) 548–563.
[15] A. Martini, E. Borfecchia, K.A. Lomachenko, I.A. Pankin, C. Negri, G. Berlier, P. Beato, H. Falsig, S. Bordiga, C. Lamberti, Composition-driven Cu-speciation and reducibility in Cu-CHA zeolite catalysts: a multivariate XAS/FTIR approach to complexity, Chem. Sci. 8 (2017) 6836–6851.
[16] A. Godiksen, F.N. Stappen, P.N.R. Vennestrøm, F. Giordanino, S.B. Rasmussen, L. F. Lundegaard, S. Mossin, Coordination environment of copper sites in Cu-CHA zeolite investigated by electron paramagnetic resonance, J. Phys. Chem. C 118 (2014) 23126–23138.

[17] V.L. Sushkevich, J.A. van Bokhoven, Revisiting copper reduction in zeolites: the impact of autoreduction and sample synthesis procedure, Chem. Commun. 54 (2018) 7447–7450.
[18] R. Millan, P. Cnudde, V. van Speybroeck, M. Boronat, Mobility and reactivity of Cu^+ species in Cu-CHA catalysts under NH_3-SCR-NO_x reaction conditions: insights from AIMD simulations, JACS Au 1 (2021) 1778–1787.
[19] A. Shishkin, H. Kannisto, P.-A. Carlsson, H. Härelind, M. Skoglundh, Synthesis and functionalization of SSZ-13 as an NH_3-SCR catalyst, Catal. Sci. Technol. 4 (2014) 3917–3926.
[20] X. Gonze, J.M. Beuken, R. Caracas, F. Detraux, M. Fuchs, G.M. Rignanese, L. Sindic, M. Verstraete, G. Zerah, F. Jollet, M. Torrent, A. Roy, M. Mikami, P. Ghosez, J. Y. Raty, D.C. Allan, First-principles computation of material properties: the ABINIT software project, Comput. Mater. Sci. 25 (2002) 478–492.
[21] G. Kresse, D. Joubert, From ultrasoft pseudopotentials to the projector augmented-wave method, Phys. Rev. B 59 (1999) 1758–1775.
[22] S. Grimme, J. Antony, S. Ehrlich, H. Krieg, A consistent and accurate ab initio parametrization of density functional dispersion correction (DFT-D) for the 94 elements H-Pu, J. Chem. Phys. 132 (2010), 154104.
[23] A.K. Rappe, C.J. Casewit, K.S. Colwell, W.A. Goddard, W.M. Skiff, UFF, a full periodic table force field for molecular mechanics and molecular dynamics simulations, J. Am. Chem. Soc. 114 (1992) 10024–10035.
[24] A.K. Rappe, W.A. Goddard, Charge equilibration for molecular dynamics simulations, J. Phys. Chem. 95 (1991) 3358–3363.
[25] A.V. Krukau, O.A. Vydrov, A.F. Izmaylov, G.E. Scuseria, Influence of the exchange screening parameter on the performance of screened hybrid functionals, J. Chem. Phys. 125 (2006), 224106.
[26] G. Kresse, J. Furthmüller, Efficiency of ab-initio total energy calculations for metals and semiconductors using a plane-wave basis set, Comput. Mater. Sci. 6 (1996) 15–50.
[27] J.P. Perdew, K. Burke, M. Ernzerhof, Generalized gradient approximation made simple, Phys. Rev. Lett. 77 (1996) 3865–3868.
[28] Y. Mao, Z. Wang, H.-F. Wang, P. Hu, Understanding catalytic reactions over zeolites: a density functional theory study of selective catalytic reduction of NO_x by NH_3 over Cu-SAPO-34, ACS Catal. 6 (2016) 7882–7891.
[29] J.H. Kwak, J.H. Lee, S.D. Burton, A.S. Lipton, C.H.F. Peden, J. Szanyi, A common intermediate for N_2 formation in enzymes and zeolites: side-on Cu–nitrosyl complexes, Angew. Chem., Int. Ed. 52 (2013) 9985–9989.
[30] J. Szanyi, J.H. Kwak, H. Zhu, C.H.F. Peden, Characterization of Cu-SSZ-13 NH_3-SCR catalysts: an in situ FTIR study, Phys. Chem. Chem. Phys. 15 (2013) 2368–2380.
[31] Y. Kuroda, M. Iwamoto, Characterization of cuprous ion in high silica zeolites and reaction mechanisms of catalytic NO decomposition and specific N_2 adsorption, Top. Catal. 28 (2004) 111–118.
[32] J.H. Kwak, T. Varga, C.H.F. Peden, F. Gao, J.C. Hanson, J. Szanyi, Following the movement of Cu ions in a SSZ-13 zeolite during dehydration, reduction and adsorption: a combined in situ TP-XRD, XANES/DRIFTS study, J. Catal. 314 (2014) 83–93.
[33] Y. Ma, X. Wu, L. Liu, L. Cao, R. Ran, Z. Si, F. Gao, D. Weng, Critical roles of Cu $(OH)_2$ in low-temperature moisture-induced degradation of Cu-SAPO-34 SCR catalyst: correlating reversible and irreversible deactivation, Appl. Catal. B Environ. 278 (2020), 119306.
[34] K. Hadjiivanov, J. Saussey, J.L. Freysz, J.C. Lavalley, FT-IR study of NO+O_2 Co-adsorption on H-ZSM-5: re-assignment of the 2133 cm^{-1} band to NO^+ species, Catal. Lett. 52 (1998) 103–108.
[35] R. Zhang, J.-S. McEwen, M. Kollár, F. Gao, Y. Wang, J. Szanyi, C.H.F. Peden, NO chemisorption on Cu/SSZ-13: a comparative study from infrared spectroscopy and DFT calculations, ACS Catal. 4 (2014) 4093–4105.
[36] F. Gao, Y. Wang, N.M. Washton, M. Kollár, J. Szanyi, C.H.F. Peden, Effects of alkali and alkaline earth cocations on the activity and hydrothermal stability of Cu/SSZ-13 NH_3–SCR catalysts, ACS Catal. 5 (2015) 6780–6791.
[37] D. Wang, L. Zhang, K. Kamasamudram, W.S. Epling, In situ-DRIFTS study of selective catalytic reduction of NO_x by NH_3 over Cu-exchanged SAPO-34, ACS Catal. 3 (2013) 871–881.
[38] R. Millan, P. Cnudde, A.E.J. Hoffman, C.W. Lopes, P. Concepción, V. van Speybroeck, M. Boronat, Theoretical and spectroscopic evidence of the dynamic nature of copper active sites in Cu-CHA catalysts under selective catalytic reduction (NH_3–SCR–NO_x) conditions, J. Phys. Chem. Lett. 11 (2020) 10060–10066.
[39] V.L. Sushkevich, A.V. Smirnov, J.A. van Bokhoven, Autoreduction of copper in zeolites: role of topology, Si/Al ratio, and copper loading, J. Phys. Chem. C 123 (2019) 9926–9934.
[40] V.V. Mesilov, S.L. Bergman, S. Dahlin, Y. Xiao, S. Xi, M. Zhirui, L. Xu, W. Chen, L. J. Pettersson, S.L. Bernasek, Differences in oxidation-reduction kinetics and mobility of Cu species in fresh and SO_2-poisoned Cu-SSZ-13 catalysts, Appl. Catal. B Environ. 284 (2021), 119756.
[41] M. Signorile, E. Borfecchia, S. Bordiga, G. Berlier, Influence of ion mobility on the redox and catalytic properties of Cu ions in zeolites, Chem. Sci. 13 (2022) 10238–10250.
[42] P. Chen, M. Jabłońska, P. Weide, T. Caumanns, T. Weirich, M. Muhler, R. Moos, R. Palkovits, U. Simon, Formation and Effect of NH_4^+ Intermediates in NH_3–SCR over Fe-ZSM-5 Zeolite Catalysts, ACS Catal. 6 (2016) 7696–7700.
[43] P. Chen, V. Rizzotto, A. Khetan, K. Xie, R. Moos, H. Pitsch, D. Ye, U. Simon, Mechanistic understanding of Cu-CHA catalyst as sensor for direct NH_3-SCR monitoring: the role of Cu mobility, ACS Appl. Mater. Interfaces 11 (2019) 8097–8105.
[44] A. Guo, K. Xie, H. Lei, V. Rizzotto, L. Chen, M. Fu, P. Chen, Y. Peng, D. Ye, U. Simon, Inhibition effect of phosphorus poisoning on the dynamics and redox of Cu active sites in a Cu-SSZ-13 NH_3-SCR catalyst for NO_x reduction, Environ. Sci. Technol. 18 (2021) 12619–12629.
[45] P. Chen, D. Rauch, P. Weide, S. Schönebaum, T. Simons, M. Muhler, R. Moos, U. Simon, The effect of Cu and Fe cations on NH_3-supported proton transport in $DeNO_x$-SCR zeolite catalysts, Catal. Sci. Technol. 6 (2016) 3362–3366.
[46] U. Simon, U. Flesch, Cation-cation interaction in dehydrated zeolites X and Y monitored by modulus spectroscopy, J. Porous Mater. 6 (1999) 33–40.
[47] P. Chen, J. Simböck, S. Schönebaum, D. Rauch, T. Simons, R. Palkovits, R. Moos, U. Simon, Monitoring NH_3 storage and conversion in Cu-ZSM-5 and Cu-SAPO-34 catalysts for NH_3-SCR by simultaneous impedance and DRIFT spectroscopy, Sens. Actuators B Chem. 236 (2016) 1075–1082.
[48] P. Chen, R. Moos, U. Simon, Metal loading affects the proton transport properties and the reaction monitoring performance of Fe-ZSM-5 and Cu-ZSM-5 in NH_3-SCR, J. Phys. Chem. C 120 (2016) 25361–25370.
[49] M.E. Franke, U. Simon, Solvate-supported proton transport in zeolites, ChemPhysChem 5 (2004) 465–472.
[50] K. Khivantsev, J.-H. Kwak, N.R. Jaegers, I.Z. Koleva, G.N. Vayssilov, M. A. Derewinski, Y. Wang, H.A. Aleksandrov, J. Szanyi, Identification of the mechanism of NO reduction with ammonia (SCR) on zeolite catalysts, Chem. Sci. 13 (2022) 10383–10394.
[51] A. Huerland, C. Plog, R. Moos, U. Simon, Amperometric measurements with a nitrosyl cation conducting ceramic membrane, Phys. Chem. Chem. Phys. 5 (2003) 5199–5202.